Shallow water sloshing modeled through the δ-SPH scheme

Matteo Antuono, Benjamin Bouscasse
CNR-INSEAN (the Italian Ship Model Basin)
Rome, Italy

Andrea Colagrossi, Claudio Lugni
CNR-INSEAN (the Italian Ship Model Basin), Rome, Italy
CESOS (Centre of Excellence for Ship and Ocean Structures)
NTNU, Trondheim, Norway

***Abstract*—The δ-SPH scheme proposed in Antuono et al. [1] has been applied to the analysis of sloshing phenomena (i.e. violent fluid motions inside a tank) in shallow water regimes. The study of such motions is of fundamental importance for the stability and structural safety of Liquid Natural Gas carriers. In this context, sloshing phenomena in shallow water represent a very demanding problem for both numerical schemes and theoretical models because of the major role played by nonlinearities. To assess the accuracy of the δ-SPH scheme, comparisons have been made with experimental measurements and with an analytical model. In all the considered cases, the δ-SPH scheme, the experiments and the analytical model display a good agreement. This further confirms the ability of the δ-SPH scheme in the modeling of violent free surface motions.**

I. Introduction

The sloshing phenomenon indicates the fluid motion inside a tank induced by external forces. It is particularly important for Liquid Natural Gas carriers and, in general, for ships which transport fluids. In fact, during the largest part of the ship travel, tanks used for the fluid/gas storage are only partially filled and the external sea motion can induce violent fluid motions inside them. Specifically, when the frequency spectrum of the ship motion is peaked in the region close to the lowest natural tank mode, violent free-surface flows may appear, inducing large local loads (see Faltinsen et al. [2]) and increasing the risk for the integrity of the structure.

For a complete description of the sloshing phenomenon it is, therefore, necessary a numerical scheme which can describe complex free surface flows (including fragmentation and wave breaking) and which can accurately predict the pressure loads against the tank walls. In this context, the SPH scheme has proved to be a reliable choice (see, for example, [3]–[6]) thanks to its Lagrangian structure and to the absence of any computational grid.

The aim of the present work is to add a further contribution to the modeling of sloshing phenomena through SPH schemes. Specifically, we adopt the δ-SPH scheme proposed in Antuono et al. [1] and further inspected in Antuono et al. [7] for gravity wave propagation. This scheme has proved to be very accurate in both the description of the free surface evolution and to the prediction of the local loads against structures.

In the present work, we deal with sloshing phenomena in shallow water conditions since they represent a very demanding problem for both numerical schemes and theoretical models because of the major role played by nonlinearities. To assess the accuracy of the δ-SPH scheme, comparisons have been made with experimental measurements and with an analytical model. In the former case, the experimental campaign of Lepelletier & Raichlen [8] and the experimental data available at the INSEAN on the shallow-water sway motion of a rectangular tank has been considered. For what concerns the comparison with the analytical model, a modal system based on depth-integrated equations (Boussinesq-type equations with a linear dispersive term) has been adopted.

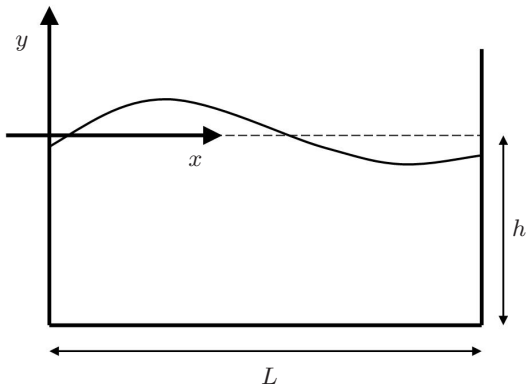

Fig. 1. Sketch of the tank and of the frame of reference.

In all the cases/experiments which follow, a rectangular tank is used and the frame of reference is set like in figure 1. Specifically, L and D indicate the tank length and breath respectively, h the filling height and $k = \pi/L$ the wave length.

II. δ-SPH scheme

The δ-SPH scheme is based on the assumption that the fluid is barotropic and weakly-compressible. Te reference equations for the flow evolution are the Euler equations along with a linear state equation. A proper artificial diffusive term is used into the continuity equation in order to remove the spurious numerical high-frequency oscillations in the pressure field and, similarly to the largest part of the weakly-compressible SPH schemes, an artificial viscous term is added inside the momentum equation for stability reasons (see for example

Monaghan [9]). The δ-SPH scheme reads:

$$\begin{cases} \dfrac{D\rho_i}{Dt} = -\rho_i \sum_j (\boldsymbol{u}_j - \boldsymbol{u}_i)\cdot\nabla_i W(\boldsymbol{r}_j)\, V_j + \\ \qquad\qquad +\delta\,\epsilon\, c_0 \sum_j \boldsymbol{\psi}_{ij}\cdot\nabla_i W(\boldsymbol{r}_j)\, V_j\,, \\ \rho_i \dfrac{D\boldsymbol{u}_i}{Dt} = -\sum_j (p_j + p_i)\,\nabla_i W(\boldsymbol{r}_j)\, V_j \;+\; \rho_i\,\boldsymbol{f}_i + \\ \qquad\qquad +\alpha\,\epsilon\, c_0\,\rho_0 \sum_j \pi_{ij}\,\nabla_i W(\boldsymbol{r}_j)\, V_j \\ p_i = c_0^2\,(\rho_i - \rho_0)\,, \\ \dfrac{D\boldsymbol{r}_i}{Dt} = \boldsymbol{u}_i\,, \end{cases} \tag{II.1}$$

where ρ_i, p_i and $\boldsymbol{u}_i$ are the density, the pressure and the velocity of the i-th particle while ρ_0 and c_0 are the density at the free surface and the sound velocity. Symbol ϵ indicates the smoothing length while $\boldsymbol{f}_i$ denotes the body force acting on the i-th particle in the frame of reference of the tank. The arguments of the diffusive and viscous terms are:

$$\boldsymbol{\psi}_{ij} = 2\,(\rho_j - \rho_i)\,\frac{(\boldsymbol{r}_j - \boldsymbol{r}_i)}{|\boldsymbol{r}_j - \boldsymbol{r}_i|^2} - \left[\,\langle\nabla\rho\rangle_i^L + \langle\nabla\rho\rangle_j^L\,\right]\,,$$

$$\pi_{ij} = \frac{(\boldsymbol{u}_j - \boldsymbol{u}_i)\cdot(\boldsymbol{r}_j - \boldsymbol{r}_i)}{|\boldsymbol{r}_j - \boldsymbol{r}_i|^2}\,.$$

The symbol $\langle\nabla\rho\rangle_i^L$ indicates that the gradient has been evaluated through a Moving Least Square interpolator (MLS hereinafter) (see Fries & Matthies [10] for more details). In all simulations, $\delta = 0.1$ while α changes according to the kinematic viscosity used in the SPH scheme. As shown in Monaghan [9], the kinematic viscosity for two-dimensional problems is $\nu_{sph} = \alpha\,\epsilon\, c_0/8$.

To reduce the computational effort, it is a common practice in the weakly-compressible SPH solvers to use a sound velocity much smaller than the physical one, generally, one order of magnitude larger than the maximum expected velocity of the fluid. However, for gravity waves the flow velocity is generally small while the most important quantity associated with the wave propagation is the wave celerity, that is, $c^2 = g/k\tanh(kh)$ (see, for example, Madsen & Shäffer [11]). For kh going to zero, the shallow water regime is approached and the relation above becomes $c^2 = gh$. Since the latter expression is an upper bound for the wave celerity (that is $g/k\tanh(kh) \leq gh$), we choose $c_0 = 10\sqrt{g\,h}$.

The detection of the free surface has been obtained through the algorithm proposed by Marrone et al. [12] while the solid boundaries have been modeled through the fixed ghost particles as described in Marrone et al. [13]. In the specific, a free slip condition has been implemented along solid boundaries and the Neumann condition has been imposed, that is $\partial p/\partial n = \rho\,\boldsymbol{f}\cdot\boldsymbol{n}$ where $\boldsymbol{n}$ is the normal unit vector to the solid profile pointing out of the fluid region.

As verified in Antuono et al. [7], the damping coefficient of the SPH scheme with free-slip conditions along solid boundaries is given by $\beta_{sph} = 4\,\nu_{sph}\,k^2$. This term has been derived from the works of Lamb [14] and Lighthill [15] under the assumption that the dissipation due to the boundary layer is negligible. Conversely, if the action of the boundary layer is accounted for, the correct damping coefficient for the n-th mode of the sloshing motion is that given by Keulegan [16]:

$$\beta_n \;=\; \sqrt{\frac{n\,k\,c\,\nu}{2}}\left(\frac{2\,h + D}{h\,D}\right) \;+\; 4\,\nu\,n^2\,k^2\,, \tag{II.2}$$

where ν is the kinematic viscosity of the fluid and c is the shallow water celerity, that is, $c = \sqrt{g\,h}$. The first term in the right-hand side of (II.2) takes into account the dissipation due to the boundary layers while the second one describes the dissipation inside the fluid bulk.

Since the structure of the SPH damping coefficient is intrinsically different from (II.2), the SPH can only approximately model the dissipation due to boundary layer. However, a good approximation is to require that the order of magnitude of β_{sph} is similar to that of β_1 (that is β_n with $n = 1$). Generally, a proper choice is $\beta_{sph} \simeq 0.2\,\beta_1$. This approximation leads to the specific choice for the SPH viscosity (that is, ν_{sph}).

III. Shallow Water Sloshing

A. Experimental set-up

The tank used during the experimental campaign at INSEAN is $L = 1$ m long, $D = 0.1$ m wide and is filled with water up to a height h. To ensure a purely sinusoidal motion, $A\sin(2\pi t/T)$ along the longitudinal direction, an *ad hoc* mechanical system has been used. Here A is the displacement amplitude and T is the period of the prescribed motion. The geometry of the tank, *i.e.* $D/L = 0.1$, ensures an almost-2D flow in the main tank plane.

Two capacitance wave probes are placed at the sides of the tank. The first one η_1 is positioned at a distance of 1 cm from one side, the second one η_2 at distance of 5 cm. During the tests, flow visualizations were performed through low- and high-speed digital video cameras. In particular, a low-speed camera (JAI CV-M2) with spatial resolution 1600x1200 pixels and frequency rate equal to 15 Hz was placed in front of the tank and sufficiently far from it to record the global behavior of the wave propagating. Further, a high-speed camera was placed closer to the front wall. Finally, a wire potentiometer was used for a direct measurement of the position of the tank. Particular care has been devoted to the synchronization of the several acquisition systems with different sampling rates, used for the recording of the signals. A suitable synchronizer has been used to trigger the start of the several acquisition systems at the selected time instants.

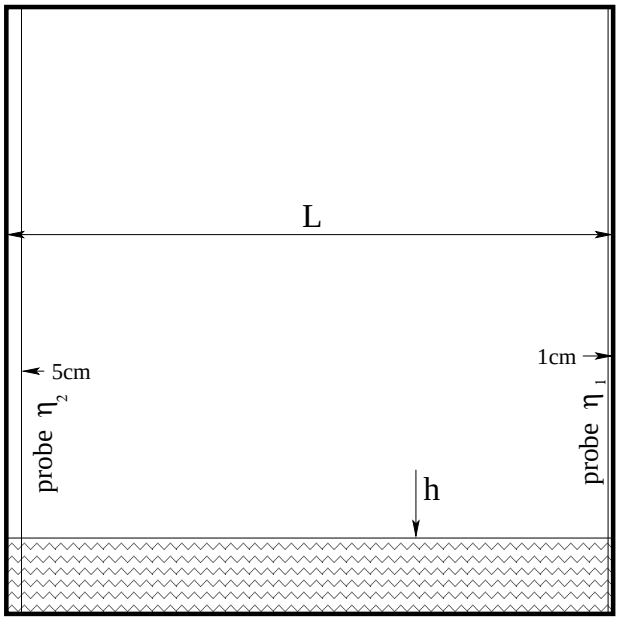

Fig. 2. sketch of the tank and probes used during the experimental campaign at INSEAN.

B. Modal system

In the shallow water regime depth-averaged models are widely used and well-established. Specifically, assuming that the tank is subjected to a generic two-dimensional time-dependent force, the following Boussinesq equations with a linearized dispersive term (see, for example, Veeramony & Svendsen [17]) can be used:

$$\begin{cases} \eta_t \,+\, h\,u_x \,+\, (\eta\,u)_x \,=\, 0 \\ \\ u_t \,+\, u\,u_x \,-\, F_2(t)\,\eta_x \,-\, \dfrac{h^2}{3}\,u_{xxt} \,=\, F_1(t)\,, \end{cases} \tag{III.3}$$

where η is the free-surface elevation, u the fluid velocity, g is the gravity acceleration while F_1 and F_2 are the horizontal and the vertical components of the global force on the tank. At the right and left walls of the tank, the impermeability condition has to be imposed, that is:

$$u(0,t) \,=\, u(L,t) \,=\, 0 \qquad \forall\, t \geq 0\,, \tag{III.4}$$

and, because of the mass conservation, the following condition must hold true:

$$\int_0^L \eta(x,t)\,dx \,=\, 0 \qquad \forall t\,. \tag{III.5}$$

If waves are non-breaking, conditions (III.4) and (III.5) are satisfied by using the following decomposition:

$$\begin{cases} \eta(x,t) = \displaystyle\sum_{n=1}^{+\infty} H_n(t)\,\cos(n\,k\,x)\,, \\ \\ u(x,t) = \displaystyle\sum_{n=1}^{+\infty} U_n(t)\,\sin(n\,k\,x)\,, \end{cases} \tag{III.6}$$

where $H_0 = U_0 = 0$, $k = 2\pi/\lambda$ and $\lambda = 2\,L$. This approach is somehow similar to the work of Hill [18] even if the series in (III.6) rely only on a spatial decomposition of the water fields, i.e., they are Fourier series in the x-variable. Since no further assumptions are made on the mode structures (that is, no specific hypotheses are made about the dependence of U_n and H_n on time), the expressions in (III.6) can be regarded as a generalization of the Hill's model.

Since the decomposition in (III.6) does not allow a straightforward inclusion of the forcing term F_1 inside the momentum equation, a proper spatial modulation $M(x)$ is introduced as follows:

$$\begin{cases} \eta_t \,+\, h\,u_x \,+\, (\eta\,u)_x \,=\, 0 \\ \\ u_t \,+\, u\,u_x \,-\, F_2(t)\,\eta_x \,-\, \dfrac{h^2}{3}\,u_{xxt} \,=\, M(x)\,F_1(t)\,. \end{cases} \tag{III.7}$$

The modulating term has is built accordingly to the decompositions in (III.6) and to the boundary conditions (III.4). Further, it has to satisfy the conservation of the momentum and of the energy associated with system (III.3) and it must approximate unity, that is $M(x) \simeq 1$. This implies:

$$M(x) = \sum_{n=1}^{+\infty} M_n\,\sin(n\,k\,x) \tag{III.8}$$

with

$$M_n \,=\, -\,2\,\left[\frac{(-1)^n - 1}{n\,\pi}\right] \quad \text{for } n \in \mathbb{Z}\backslash\{0\}\,, \tag{III.9}$$

and $M_0 = 0$. Substituting (III.6) and (III.8) into (III.7), we get a system of $2 \times N$ ordinary differential equations for H_n and U_n with $n = 1, 2 \ldots N$ (N is the number of modes considered for the simulation). Similarly to the works of Hill [18] and Faltinsen & Timokha [19], a linear viscous term (i.e., a term that is proportional to the fluid velocity) is added to the equation for U_n. The coefficient of the viscous term (that is, the damping coefficient) is given by the expression (II.2) for β_n.

C. Sway motion

Sway motion consists of a horizontal forcing while the vertical displacement and rotation are null.

We first consider the experimental campaign made by Lepelletier & Raichlen [8] where two different configurations were considered. In the first case, the tank dimensions are $L = 117.5cm$, $D = 12cm$ and the still water level is $h = 6cm$ The first resonant frequency predicted through the linear theory is $\omega_r = 2.04s^{-1}$, the horizontal forcing law is sinusoidal and its amplitude is $A_1 = 0.39cm$. The kinematic viscosity is $\nu = 0.0094cm^2/s$.

Figure 3 displays the comparison between the experiments by Lepelletier & Raichlen [8] (triangles and thin solid line) and the δ-SPH scheme (diamonds and thin solid line) for the steady-state maximum wave elevation at the right wall of the tank ($x/L = 1$). The overall agreement is very good and the bifurcation predicted by the present model is close to that

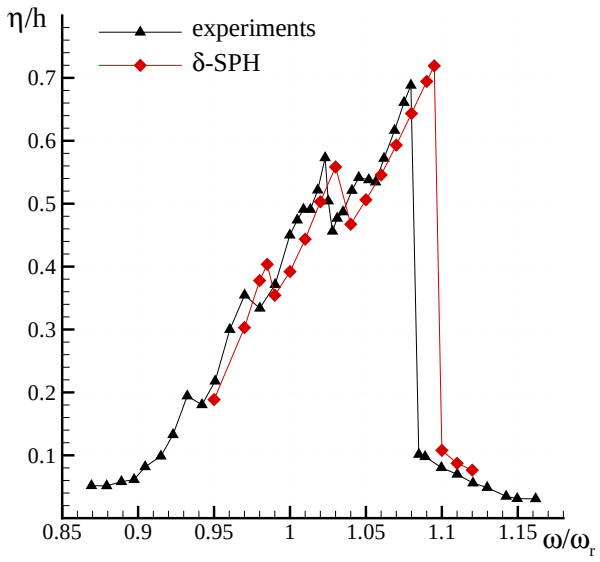

Fig. 3. Sway motion, response amplitude operator at $x/L = 1$ for the first configuration of Lepelletier & Raichlen [8] ($h/L = 0.051$, $A/h = 0.065$).

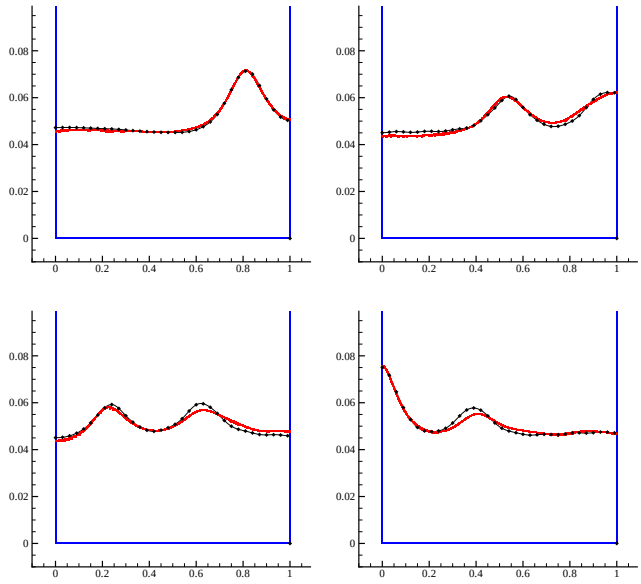

Fig. 4. Snapshots of the free surface evolution for the first configuration of Lepelletier & Raichlen [8] ($h/L = 0.051$, $A/h = 0.065$, $\omega/\omega_r = 1.02$). Black diamonds indicate the analytical solution obtained through the modal system.

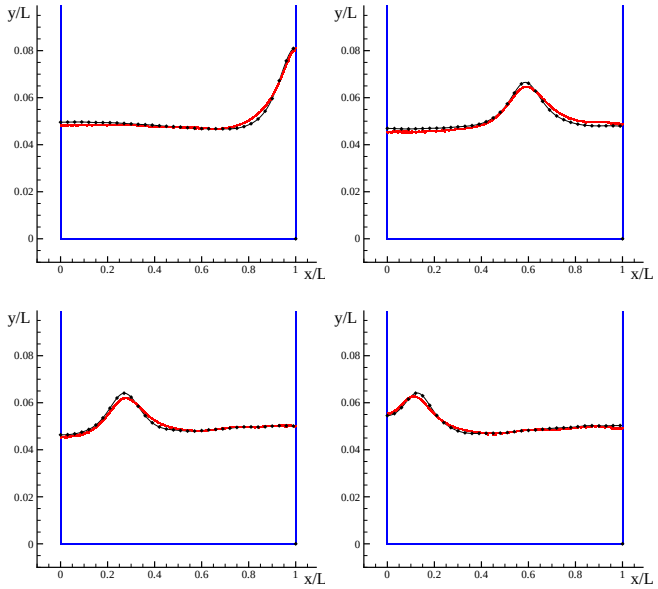

Fig. 5. Snapshots of the free surface evolution for the first configuration of Lepelletier & Raichlen [8] ($h/L = 0.051$, $A/h = 0.065$, $\omega/\omega_r = 1.08$). Black diamonds indicate the analytical solution obtained through the modal system.

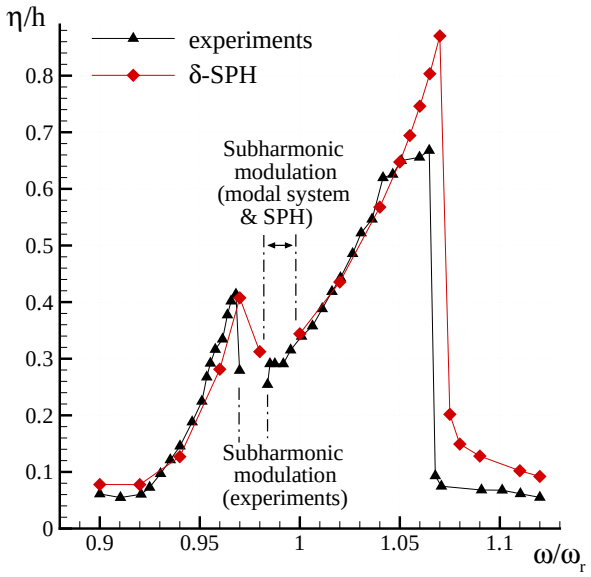

Fig. 6. Sway motion, response amplitude operator at $x/L = 1$ for the second configuration of Lepelletier & Raichlen [8] ($h/L = 0.098$, $A/h = 0.033$).

shown by the experiments even if the δ-SPH scheme tends to slightly delay the bifurcation point. The adopted viscosity for the δ-SPH scheme is $\nu_{sph} = 2.4 \cdot 10^{-4} m^2/s$.

The small peaks that appear along the left branch of the response amplitude operator (see figure 3) correspond to the boundaries of different regimes of the sloshing evolution. Each regime is characterized by a specific number of waves and this number decreases as the peaks approach the bifurcation point (see, for example, Olsen & Johnsen [20]). The last regime before the bifurcation is characterized by a solitary wave that moves back and forth in the basin. After the bifurcation, only one wave is observed. Figures 4 and 5 display the free surface elevation for some of these regimes. These results have been compared with the modal system described in Section III-B showing an excellent match.

The second configuration considered by Lepelletier & Raichlen [8] is particularly demanding for it is characterized by $h/L = 0.098$ and, therefore, is very close to the intermediate water regime. Lepelletier and Raichlen observed the occurrence of wave breaking during the transient evolution

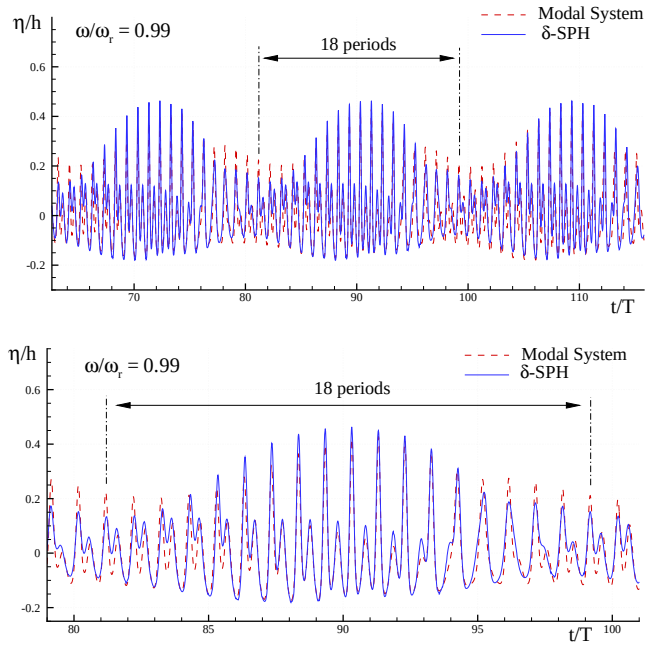

Fig. 7. Evolution of the free surface at $x/L = 0.95$ for the second configuration of Lepelletier & Raichlen [8] ($h/L = 0.098$, $A/h = 0.033$, $\omega/\omega_r = 0.99$)..

of those cases characterized by frequencies just to the left of the bifurcation point (that is, $\omega/\omega_r = 1.06$). However, no breaking was observed at the steady state. This implies that the comparison with the modal system of Section III-B is still allowed. Indeed, since the modal system cannot describe wave breaking, this leads to an excess of energy during the transitory which just corresponds to a delay in the attainment of the steady state.

Figure 6 displays the comparison between the amplitude response operator at $x/L = 1$ as given by the experimental measures (triangles and thin solid line) and by the δ-SPH scheme (diamonds and thin solid line). The overall match is very good and the bifurcation point is predicted with a fair accuracy. Here, the viscosity of the δ-SPH scheme is $\nu_{sph} = 6.5 \cdot 10^{-5} m^2/s$.

In this case only two regimes are observed before the bifurcation point: a two-wave regime and a solitary-wave regime. Between these regimes a special region of motion was detected during the experimental campaign. In that region no steady state was attained and a nonlinear subharmonic modulation of 18 periods was observed (see Lepelletier & Raichlen [8]). Remarkably, both the δ-SPH scheme and the modal system predict the same modulation in a region very close to that shown by the experiments (see figure 6). Details on the nonlinear beating phenomenon are provided in figure 7 and are compared with the modal system. In this case, very long simulations have been performed to ensure the attainment of a periodic asymptotic solution. Again, the agreement between the numerical and theoretical model is very good.

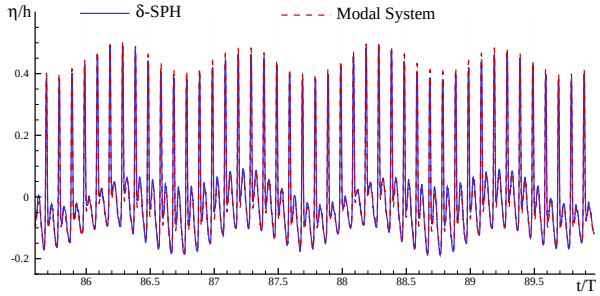

Fig. 8. Free surface elevation at $x/L = 0.95$ for the general 2D motion described in Section III-D

D. General 2D motion

To prove that the δ-SPH scheme is capable to describe a sloshing flow excited by a generic two-dimensional motion, we consider a problem in which sway, roll and heave motion are involved. The tank dimensions and filling height are the same of the first configuration used by Lepelletier & Raichlen and the tank motion is given by:

$$x(t) = A_1 \sin(\omega_1 t + \phi_1) \qquad y(t) = A_2 \sin(\omega_2 t + \phi_2)$$

$$\theta(t) = \theta_0 \sin(\omega_0 t + \phi_0) \, ,$$

where $A_1 = 0.006m, \omega_1 = 2.2s^{-1}, \phi_1 = 0$ (sway motion), $A_2 = 0.03m, \omega_2 = 4.29s^{-1}, \phi_2 = 0$ (heave motion) and $\theta_0 = \pi/720\, rad, \omega_0 = 0.22s^{-1}, \phi_0 = 0$ (roll motion). The axis of rotation is placed at $\boldsymbol{r}_0 = (L/2, 0)$. To avoid an impulsive start and make the motion more general, we introduce a polynomial ramp during the early stages of the tank evolution. This is given by:

$$r(\tau) = \tau^3 \left(6\,\tau^2 - 15\,\tau + 10 \right) , \qquad \text{(III.10)}$$

where $\tau = (t - t_0^{(r)})/\Delta t$, $t_0^{(r)}$ is the instant when the ramp is firstly applied ($t_0^{(r)}$ has been set equal to the initial time of the simulation) and Δt is the ramp duration (here $\Delta t = 2\pi/\omega_0$). The polynomial ramp satisfies:

$$r(0) = \dot{r}(0) = \ddot{r}(0) = 0 \qquad r(1) = 1 \qquad \dot{r}(1) = \ddot{r}(1) = 0 \, ,$$

so that the initial application of the ramp and its transition towards the imposed motion is perfectly smooth. Similarly to the first case of sway motion, the SPH viscosity is set equal to $2.4 \cdot 10^{-4} m^2/s$. Since no comparisons with experiments are available for this case, we use the analytical model described in Section III-B to get a reference solution.

In figure 8 the free surface evolution at $x/L = 0.95$ is displayed. The time history clearly shows different periods of oscillations induced by the nonlinear interaction of the components of the tank motion (that is, sway, roll and heave). The comparison with the modal system is very good. Similarly, figure 9 displays the comparison between the free surface predicted through the δ-SPH and the modal system. Here, the match is slightly worse with respect to the sway cases described in Section III-C. In any case, apart from small discrepancies, the global wave pattern is well predicted. This is

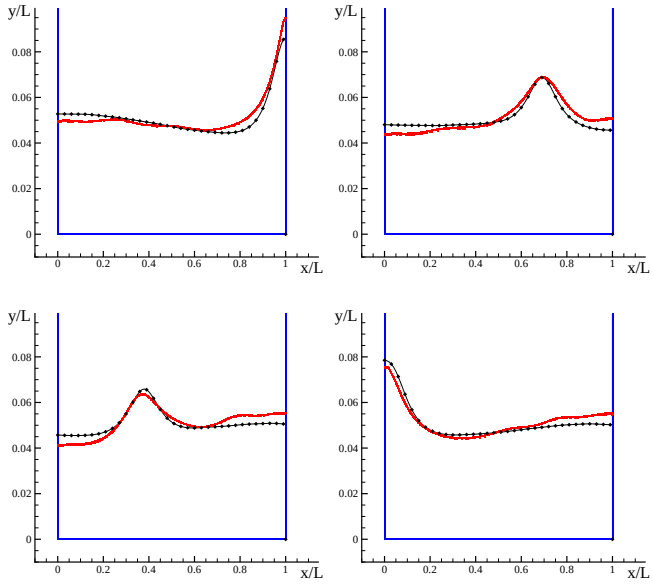

Fig. 9. Snapshots of the free surface evolution for the general 2D motion described in Section III-D. Black diamonds indicate the analytical solution obtained through the modal system.

a relevant results since the sloshing problem at hand involves both sway, heave and roll motion and, therefore, represents a very demanding test.

E. Experiments at INSEAN

Here we consider a specific case of sway motion taken from the large amount of data available at INSEAN. This is characterized by $h/L = 0.03$ and $A/L = 2.33$, that is, by a very shallow water depth and by a large horizontal forcing. For these reasons, wave breaking and splash-up events occur during the flow evolution and this case represents a very demanding test for numerical schemes.

Figures 10 and 11 display the response amplitude operators obtained at $x/L = 0.99$ and $x/L = 0.95$ respectively. Although the experimental data are a few, the agreement with the δ-SPH scheme is very good. Note that the shapes of the amplitude operators in figures 10 and 11 are quite different from those displayed in figures 3 and 6. This is due to the occurrence of wave breaking for those cases characterized by a higher response to the sway forced motion. This leads to energy dissipation and to a consequent lowering of the response operator in the neighborhood of the bifurcation point.

A further confirmation of the capability of the δ-SPH scheme to correctly predict the flow evolution is given in figures 12 and 13. There, some snapshots of the free surface evolution are displayed for $\omega/\omega_r = 1.231$ and $\omega/\omega_r = 1.319$. The δ-SPH scheme well describes wave breaking and the subsequent splash-up events.

IV. Conclusion

Using experimental data available in the literature and comparisons with a semi-analytical modal scheme, the δ-SPH has been tested against several shallow water sloshing

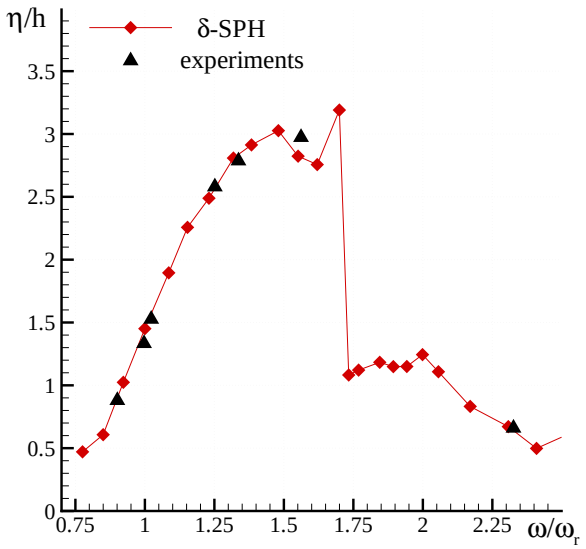

Fig. 10. Sway motion, response amplitude operator at $x/L = 0.99$ for the case described in Section III-E.

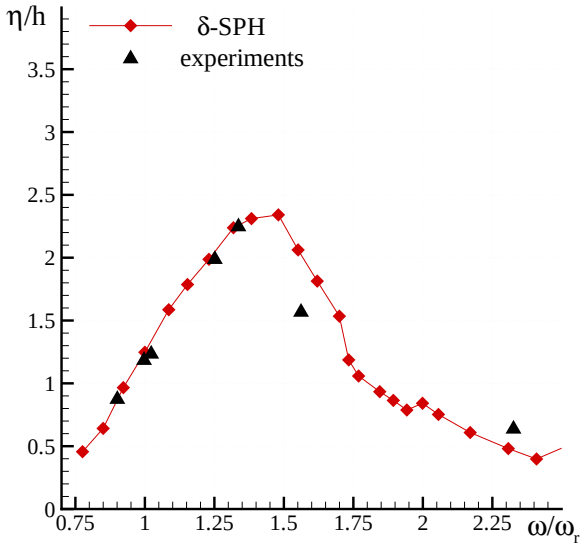

Fig. 11. Sway motion, response amplitude operator at $x/L = 0.95$ for the case described in Section III-E.

problems into a rectangular tank. Both sway motion and a generic two-dimensional motion have been considered proving that the δ-SPH is capable to predict the sloshing evolution with high accuracy even during the occurrence of wave breaking and splash-up events.

Acknowledgment

The research leading to these results has received funding from the European Community's Seventh Framework Programme (FP7/2007-2013) under grant agreement n. 225967 "NextMuSE". This work was also partially supported by the Centre of Excellence for Ship and Ocean Structures of NTNU Trondheim (Norway) within the "Violent Water-Vessel Interactions and Related".

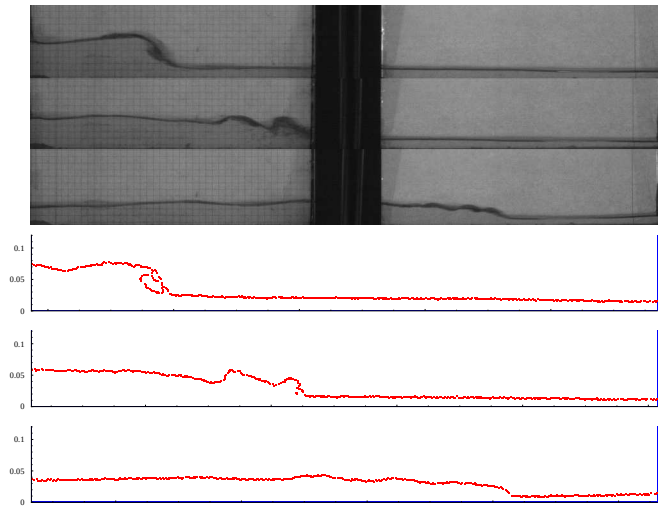

Fig. 12. Snapshots of the free surface evolution for the case described in Section III-E ($\omega/\omega_r = 1.231$). Upper panels: experiments. Lower panels: δ-SPH.

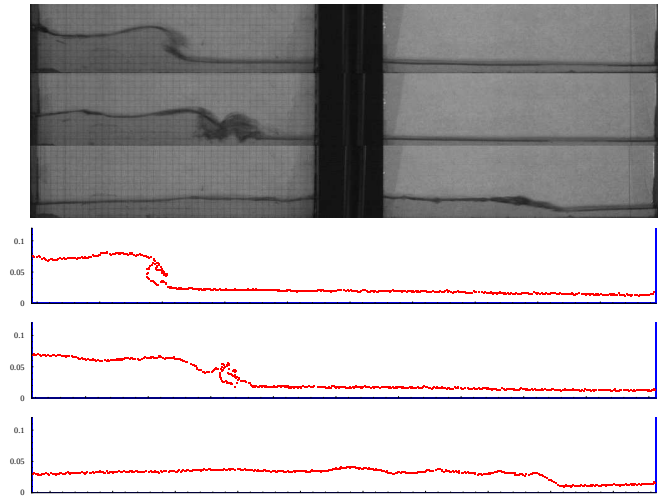

Fig. 13. Snapshots of the free surface evolution for the case described in Section III-E ($\omega/\omega_r = 1.319$). Upper panels: experiments. Lower panels: δ-SPH.

REFERENCES

[1] M. Antuono, A. Colagrossi, S. Marrone, D. Molteni, *Free-surface flows solved by means of SPH schemes with numerical diffusive terms*, Computer Physics Communications, 181(3): 532-549 (2009)

[2] O.M. Faltinsen, M. Landrini, M. Greco, *Slamming in marine applications*, J. Engng. Math. 48: 187-217 (2004)

[3] A. Colagrossi, G. Colicchio, C. Lugni, M. Brocchini, *A study of violent sloshing wave impacts using an improved SPH method*, J. Hydr. Res., 48: 94-104 (2010)

[4] A. Souto-Iglesias, L. Delorme, L. P. Pérez-Rojas, S. Abril-Pérez, *Liquid moment amplitude assessment in sloshing type problems with smooth particle hydrodynamics*, Ocean Engineering, 33(11): 1462-1484 (2006)

[5] G. Bulian, A. Souto-Iglesias, L. Delorme, E. Botia-Vera, *Smoothed particle hydrodynamics (SPH) simulation of a tuned liquid damper*, J. Hydraulic Research, 48(1): 28-39 (2010)

[6] B. Bouscasse, A. Colagrossi, G. Colicchio, C. Lugni, *Numerical and experimental investigation of sloshing phenomena in conditions of low filling ratios*, 10^{th} Numerical Towing Tank Symposium (NuTTS'07) Hamburg, Germany, 23-25 Sept., 2007

[7] M. Antuono, A. Colagrossi, S. Marrone, C. Lugni, *Propagation of gravity waves through a SPH schemes with numerical diffusive terms*, Comp. Phys. Comm., 182: 866-877 (2011)

[8] T.G. Lepelletier & F. Raichlen, *Nonlinear oscillations in rectangular tanks*, J. Engng. Maths., 114(1): 1-23 (1988)

[9] J.J. Monaghan, *Smoothed particle hydrodynamics*, Rep. Progr. Phys. 68: 1703-1759 (2005)

[10] T. P. Fries, H. G. Matthies, *Classification and overview of meshfree methods*, Informatikbericht 2003-03, Institute of Scientific Computing, Technical University Braunschweig, Brunswick, Germany (2004)

[11] P. A. Madsen and H. A. Shäffer, *A discussion of artificial compressibility*, Coast. Engng., 53: 93-98 (2006)

[12] S. Marrone, A. Colagrossi, D. Le Touzé, G. Graziani, *Fast free-surface detection and level-set definition in SPH solvers*, J. Comp. Phys., 229: 3652-3663 (2010)

[13] S. Marrone, M. Antuono, A. Colagrossi, G. Colicchio, D. Le Touzé, G. Graziani, *δ-SPH model for simulating violent impact flows*, Comput. Methods Appl. Mech. Engrg., 200: 1526-1542 (2011)

[14] H. Lamb, *Hydrodynamics*, Cambridge University Press, 1945

[15] J. Lighthill, *Waves in fluids*, Cambridge University Press, 2001

[16] G. H. Keulegan, *Energy dissipation in standing waves in rectangular basins*, J. Fluid Mech., 6: 33-50 (1959)

[17] J. Veeramony and I.A. Svendsen, *The flow in surf-zone waves*, Coast. Engng., 39: 93-122, (2000)

[18] D. F. Hill, *Transient and steady-state amplitudes of forced waves in rectangular basins*, Phys. Fluids, 39(6): 1576-1587 (2003)

[19] O. M. Faltinsen, A. N. Timokha, *An adaptive multimodal approach to nonlinear sloshing in a rectangular tank*, J. Fluid Mech., 432: 167-200 (2001)

[20] H. Olsen and K. Johnsen, *Nonlinear sloshing in rectangular tanks: a pilot study on the applicability of analytical models*, Tech. Rep., Det Norske Veritas (DNV), Hvik, Norway, 74-72-5 Vol. 2 (1975)